Tunnelling and Underground Space Technology 78 (2018) 168–177

Contents lists available at ScienceDirect

Tunnelling and Underground Space Technology

journal homepage: www.elsevier.com/locate/tust

Soil-tunnel interaction modelling for shield tunnels considering shearing dislocation in longitudinal joints

Huai-Na Wu[a,b], Shui-Long Shen[a,*], Jun Yang[c], Annan Zhou[d]

[a] State Key Laboratory of Ocean Engineering and Collaborative Innovation Center for Advanced Ship and Deep-Sea Exploration (CISSE), School of Naval Architecture, Ocean, and Civil Engineering, Shanghai Jiao Tong University, 800 Dong Chuan Road, Minhang District, Shanghai 200240, China
[b] College of Civil Engineering, Hunan University, Changsha 410082, Hunan, China
[c] Department of Civil Engineering, The University of Hong Kong, Pokfulam, Hong Kong, China
[d] School of Engineering, Royal Melbourne Institute of Technology, Victoria 3001, Australia

ARTICLE INFO

Keywords:
Shield tunnel
Soil-tunnel interaction
Timoshenko
Vlasov foundation
Shearing dislocation

ABSTRACT

The existing longitudinal structural model of shield tunnels usually simplify the tunnel as a Euler-Bernoulli beam on elastic foundation, which ignores the shearing dislocation between rings. To model the dislocation between rings, this paper proposed a soil-tunnel interaction model based on the Timoshenko beam simplified model (TBSM) of tunnel on Vlasov foundation. The governing differential equation and the closed-form solution for TBSM on Vlasov foundation subjected to any given pressure are derived with consideration of two types of boundary conditions. The proposed model was adopted to analyze the behaviors of a shield tunnel subjected to external forces transferred from surcharge load on the ground surface. Factors influencing the longitudinal behavior of shield tunnels are discussed. The factors include the equivalent of shear stiffness, location of load application, and the rotational stiffness of the joint between tunnel and station. The results indicated that Euler-Bernoulli beam model underestimates deformation and overestimates the internal forces in the tunnel structure. When the load application is close to the station, with the decrease of the distance between the load and the station will lead to a slightly decrease of the maximum settlement of the tunnel, and an increase of the maximum internal forces and the maximum joint deformation. A stiffer joint between tunnel and station will cause greater internal forces at the location of joint.

1. Introduction

Shield tunneling method has been widely utilized in soft deposits due to the following many advantages: highly safe construction efficiency, and less environmental impacts (Shen et al., 2016; Liu et al., 2018; Cheng et al, 2017b). The lining of a shield tunnel is composed of precast reinforced concrete segments connected by steel bolts (Cheng et al., 2017a). During long-term operation, shield tunnels often suffer from differential settlement to cause joint opening (Shen et al., 2014; Wu et al., 2017) and longitudinal structural deformation due to the effect of uneven subsoils, nearby construction (Chai et al., 2018), land subsidence (Shen and Xu, 2011; Shen et al., 2013), traffic loading, and groundwater leakage (Mair and Taylor, 1997; Mair, 2008; Wu et al., 2013; Huang et al., 2015). Large longitudinal deformation will inevitably result in a series of problems such as deformation of joints, cracks of concrete segments, groundwater leakages, distortion of track, which may threaten safety during train running (Shen et al., 2015; Wu et al., 2015). The differential settlement and longitudinal deformation of shield tunnels during operation has drawn more and more attention (ITA, 2000; Zhang et al., 2018).

In the last three decades, many attempts have been made to establish a soil-tunnel interaction model for longitudinal analysis (Liao et al., 2008; Huang et al., 2015; Ren et al., 2018). The most common way is to consider the tunnel/soil interaction problem as a beam structure on elastic springs, which is a one-dimensional problem. For tunnels, typical structural models include beam-spring model (Koizumi et al., 1988) and longitudinal continuous model (Shiba et al., 1988). The beam-spring model considers the ring as an one-dimensional short beam, and the joints as the spring elements to resist axial, shear forces, and rotational moment (see Fig. 1(a)). The longitudinal continuous model, however, considers the tunnel as a homogenous beam with reduction stiffness (see Fig. 1(b)). Compared with the beam-spring model, the longitudinal continuous model is much simpler in computation, making it widely used in soil-tunnel interaction analysis.

For the longitudinal continuous model, the previous studies commonly considered a tunnel as a continuous Euler-Bernoulli beam

* Corresponding author.
E-mail addresses: wuhn@hnu.edu.cn (H.-N. Wu), slshen@sjtu.edu.cn (S.-L. Shen), junyang@hku.hk (J. Yang), annan.zhou@rmit.edu.au (A. Zhou).

https://doi.org/10.1016/j.tust.2018.04.009
Received 22 March 2017; Received in revised form 2 March 2018; Accepted 8 April 2018
Available online 27 April 2018

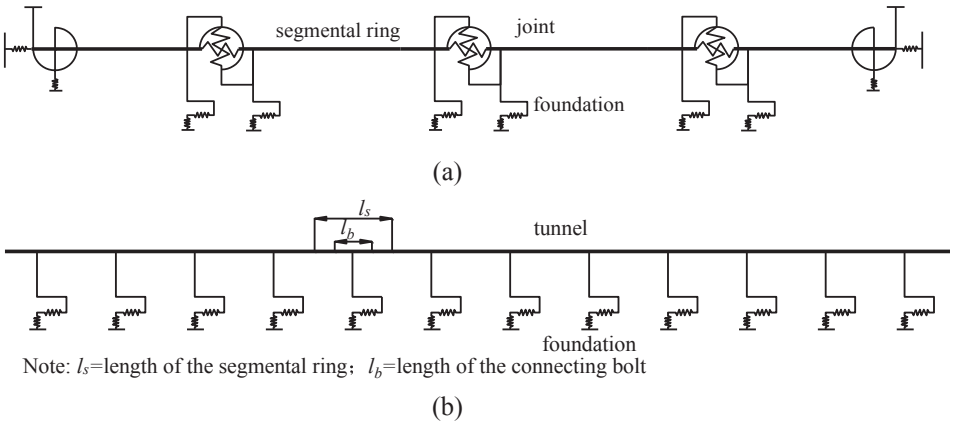

Fig. 1. Longitudinal structural model: (a) beam-spring model; (b) longitudinal continuous model.

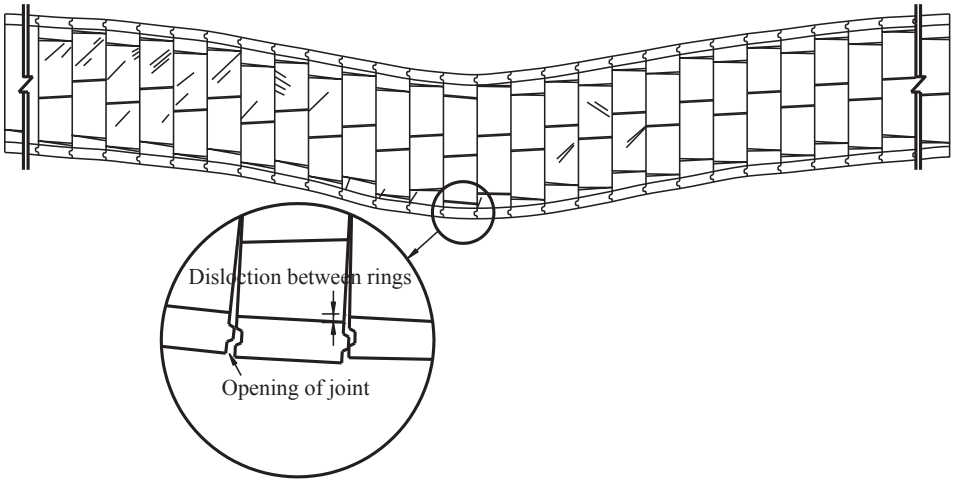

Fig.2. Longitudinal deformation of a shield-driven water pipeline in Shanghai (recreated based on the data from Liao et al., 2008).

(Bogaards and Bakker, 1999; Huang et al., 2012, 2015; Talmon and Bezuijen, 2013 Cheng et al, 2017b), which considered the longitudinal deformation as a pure bending deformation with opening of the joints. However, it is widely observed that shearing dislocation between rings occurs during long-term operation of shield tunnels (Wang, 2009; Shen et al., 2014; Wu et al., 2015). Fig. 2 shows the structural deformation of a shield-driven water pipeline in Shanghai, China. As shown in Fig. 2, the joint deformation includes both opening of joint and dislocation between rings. Such deformation reflects a flexure deformation under bending moment, and a shear deformation in longitudinal direction. The traditional Euler-Bernoulli model only accounts for flexural deformation under bending and fails to capture the shearing-induced dislocation between rings. A soil-tunnel interaction analysis based on this structural model will give inaccurate results. Wu et al. (2015) proposed a Timoshenko beam simplified model (TBSM), in which the tunnel is simplified as a continuous Timoshenko beam with equivalent flexure stiffness $(EI)_{eq}$ and shear stiffness $(\kappa GA)_{eq}$. TBSM presents the deformation behavior of shearing dislocation reasonably well. However, Wu et al. (2015) did not provide the analysis method for soil-tunnel interaction, which limits the application of TBSM.

There have been many constitutive models that attempt to simulate the actual behavior of foundation soils. However, these models are difficult to use for analytical analysis of structure/soil interaction problems due to the complex calculations involved. Therefore, some simple elastic foundation models, such as Winkler model and two-parameter models, continue to be widely used (Han and Frost, 2000; Yin, 2000a,b; Li et al., 2016). The Winkler model is the simplest representation of a foundation response. It idealizes the foundation to consist of closely spaced independent springs (Winkler, 1867). The shortcoming of this model is that it does not account for the shear strains in the ground. To address this shortcoming, some two-parameter models that are capable of considering the interaction among the discrete springs have been proposed, such as Vlasov model, Hetenyi model, Pasternak model (Vlasov and Leontev, 1966; Hetenyi, 1946; Pasternak, 1954). These models are therefore expected to better capture the soil response via selection of appropriate soil parameters (Jin et al., 2016, 2017; Yin et al., 2018).

This paper aims to establish a soil-tunnel interaction model by combining the TBSM proposed by Wu et al. (2015) with the Vlasov foundation model. A closed-form solution of a shield tunnel on Vlasov foundation subjected to arbitrary pressure loading will be derived. With the proposed model, the effect of the equivalent shear stiffness, the location of load application, and the rotational stiffness of the joint between tunnel and station on the longitudinal behavior of the tunnel structure are discussed.

2. Brief introduction of TBSM

2.1. Shearing-dislocation deformation of shield tunnels

Fig. 3 plots the modes of longitudinal deformation of a shield tunnel. The lining is a composite structure consisting of segmental rings and circumferential joints. Since the joints have a lower stiffness than the segmental rings, joint deformation is the main element causing longitudinal deformation. In view of different joint deformation types, longitudinal deformation can be identified as following two modes: *i*)

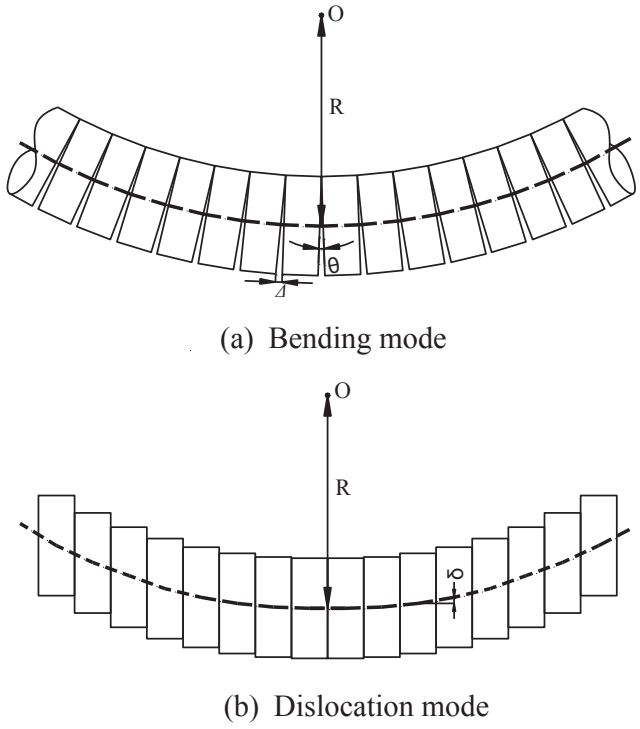

Fig. 3. Longitudinal deformation modes of shield tunnel (after Wu et al., 2015).

bending mode and *ii*) dislocation mode. In the bending mode, rings rotate around the center of deformation curve. In the dislocation mode, differential settlement of the tunnel is an accumulation of the dislocation between rings. The flexural deformation of the tunnel inevitably exists whereas the shear stiffness of the circumferential joints is relatively small, which makes the shear deformation of the whole tunnel to become a significant component of the longitudinal deformation.

2.2. Timoshenko beam simplified model

Fig. 4 shows the schematic illustration of the TBSM proposed by Wu et al. (2015). The tunnel is consisted of a series of segmental rings and joints between them in the longitudinal direction. Taking one ring and the adjacent joint as one calculation unit, the tunnel can be considered as a continuous Timoshenko beam that is made up of a series of beam elements of ring-joint units. Uniform stiffness was adopted for TBSM along the tunnel axis. Since the joint is composed of a series of bolts, it leads to an apparent stiffness reduction along the tunnel, which should be taken into account in the model.

For the TBSM, governing equations for a tunnel model can be obtained based on the Timoshenko theory (Timoshenko, 1921):

$$Q = \frac{dM}{dx},\ \frac{dQ}{dx} - q = \frac{d^2M}{dx^2} - q = 0 \tag{1a,b}$$

$$\varphi = \frac{dw}{dx} - \gamma,\ k_c = -\frac{d\varphi}{dx} = -\frac{d^2w}{dx^2} + \frac{d\gamma}{dx} \tag{2a,b}$$

$$M = (EI)_{eq}k_c,\ Q = (\kappa GA)_{eq}\gamma \tag{3a,b}$$

where Q = shear force, M = bending moment, q = applied transverse load, w = deflection of the neutral axis of the beam, φ = rotation angle of the cross section, k_c = curvature of the neutral axis; $(EI)_{eq}$ = equivalent flexural stiffness, in which E = Young's modulus, I = area moment of inertia of the cross-section; $(\kappa GA)_{eq}$ = equivalent shear stiffness, in which G = shear modulus, A = cross sectional area, κ = the coefficient of Timoshenko shear, depending on the geometry. Normally, $\kappa = 1/2$ for annular cross sections.

The stiffness reduction effect of the joints between rings was considered by using equivalent flexure stiffness $(EI)_{eq}$ and shear stiffness $(\kappa GA)_{eq}$, which obey the following deformation equivalence hypothesis: (i) under pure bending, the flexure deformation of the beam element equal to the sum of the flexure deformation of ring and joint; (ii) under pure shear force, the shear deformtion of the beam element equal to the sum of the flexure deformation of ring and joint (Wu et al., 2015). That is,

$$\theta = \theta_j + \theta_s \tag{4a}$$

$$u = u_j + u_s \tag{4b}$$

where, θ = the rotation angles displacement of the ring-joint unit; θ_j = rotation angles of the joint; θ_s = rotation angles of the segment ring; u = the equivalent shear displacement of the ring-joint unit; u_j = the shear displacement of the joint; u_s = the shear displacement of the segmental ring.

According to the coordination system and equilibrium equation, the rotation angles of the section within and beyond the influence range of the joint can be derived, which are expressed as (Liao et al., 2008):

$$\theta_j = \frac{\lambda l_b M}{K_J E_s I_s} \tag{5a}$$

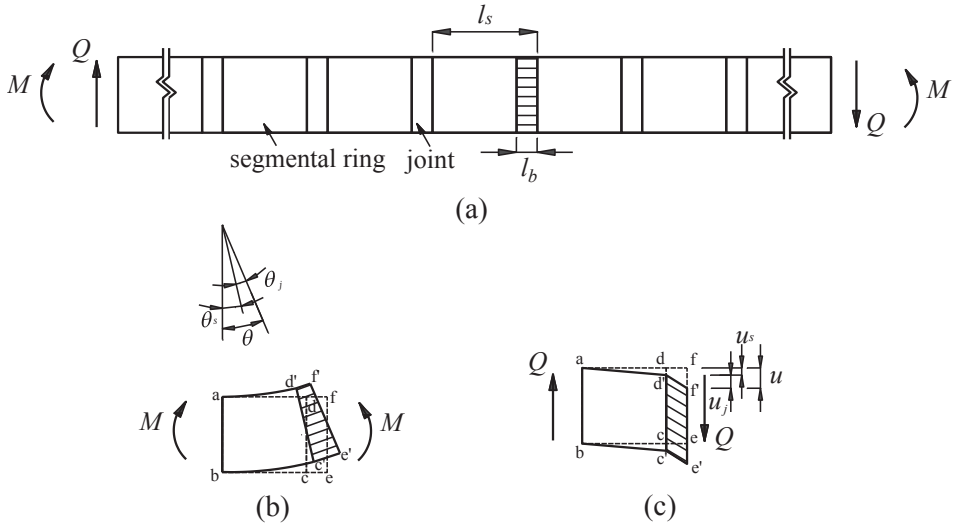

Fig. 4. Illustration of Timoshenko beam simplified model (after Wu et al., 2015).

$$\theta_s = \frac{M(l_s - \lambda l_b)}{E_s I_s} \tag{5b}$$

where, l_s = length of the segmental ring; l_b = length of the connecting bolt; E_s = Young's modulus of segment concrete; I_s = area moment of inertia of the cross-section; K_f is the coefficient of rotational stiffness of circumferential joint, which is calculated by the following equation: $K_f = \frac{\cos^3\psi}{\cos\psi + (\psi + \pi/2)\sin\psi}$, in which ψ = location of neutral axis angle (Liao et al., 2008); λ = influence factor of circumferential joints; η is the reduction factor of flexural stiffness. Substituting Eqs. (5a) and (5b) into Eq. (4a), yields (Liao et al., 2008):

$$(EI)_{eq} = E_s I_s \cdot \frac{K_f l_s}{K_f(l_s - \lambda l_b) + \lambda l_b} = \eta E_s I_s \tag{6}$$

where, η is the reduction factor of flexural stiffness.

Following the methodology of Liao et al. (2008), Wu et al. (2015) derived the equivalent shear stiffness based on Eq. (4b). The shear displacement of the joint and segmental ring can be expressed using the following formulas.

$$u_j = l_b \tan\gamma_b = l_b \tan\frac{Q}{n\kappa_b G_b A_b} \tag{7a}$$

$$u_s = (l_s - l_b)\tan\gamma_s = (l_s - l_b)\tan\frac{Q}{\kappa_s G_s A_s} \tag{7b}$$

where, γ_b = shear distortion of bolt; G_b = shear modulus of bolt; A_b = cross sectional area of bolt; κ_b = Timoshenko shear coefficient of bolt, and for a circular section, κ_b = 0.9; γ_s = shear distortion of segmental ring; G_s = Shear modulus of segmental ring; A_s = cross sectional area of segmental ring; κ_s = Timoshenko shear coefficient of segmental ring, and for an annular cross section, κ_s = 0.5. Substituting Eqs. (7a) and (7b) into Eq. (4b), the equivalent shear stiffness $(\kappa GA)_{eq}$ can be expressed as follows:

$$(\kappa GA)_{eq} = \xi \frac{l_s}{\frac{l_b}{n\kappa_b G_b A_b} + \frac{l_s - l_b}{\kappa_s G_s A_s}} \tag{8}$$

where, ξ is a modification factor introduced here to consider the influences of the friction between segments, the tongue and groove joint, and the sealing gasket.

Based on the geometrical relationship, Wu et al. (2015) derived the maximum opening of the joint Δ, which is located on the edge of the tension side, and the dislocation between the segmental rings, δ:

$$\Delta = \theta_j(r + r\sin\psi) = \frac{M\lambda l_b}{E_s I_s}\cdot\frac{1}{\zeta}\cdot(r + r\sin\psi) \tag{9}$$

$$\delta = l_s \tan\gamma = l_s \tan\frac{Q}{(\kappa GA)_{eq}} \tag{10}$$

where r = outer radius of the segmental ring, γ = shear distortion of the tunnel.

3. Soil-tunnel modelling based on TBSM

In this paper, soil response to tunnel with applied load is simulated by a Vlasov foundation. By combining the Timoshenko beam model of tunnel with Vlasov foundation theory, the interaction between soil and tunnel can be analyzed. Fig. 5(a) shows the proposed soil-tunnel interaction model, which is an equivalent Timoshenko beam on a Vlasov foundation. Fig. 5(b) shows two displacement parameters of tunnel deformation, settlement w and rotation angle φ, and the defined positive direction. Fig. 5(c) shows a tunnel element supported by soil springs with the positive direction of the forces on the element. A Timoshenko beam on the Winkler foundation has been analyzed by Han and Frost (2000) and Yin (2000a, 2000b). This paper extends his method to the analysis of Timoshenko beam on Vlasov foundation, and different boundary conditions are considered.

The vertical force equilibrium of the Timoshenko beam element in Fig. 5(c) leads to (Vlasov and Leontev, 1966):

$$\frac{dQ}{dx} = k_e w - 2t_e\left(\frac{\partial^2 w}{\partial x^2}\right) - q \tag{11}$$

where w = vertical displacement of tunnel; q = function of pressure acting on the tunnel in the longitudinal direction. $q(x) = \int_{-r}^{r} f(x,y)dy$, in $f(x,y)$ = function of pressure acting on the tunnel; k_e = equivalent compression coefficient of Vlasov foundation, t_e = equivalent shear coefficient of Vlasov foundation; $k_e = kb$, $t_e = tb$, in which, k = compression modulus of Vlasov foundation, t = shear modulus of Vlasov foundation, b = outer diamter of tunnel.

According to Eqs. (1a), (2a), (2b), (3a), (3b), the following equation can be obtained:

$$D\frac{d^2\varphi}{dx^2} - C\varphi + C\frac{dw}{dx} = 0 \tag{12}$$

where $D = (EI)_{eq}$, $C = (\kappa GA)_{eq}$. Substituting Eqs. (2a) and (3b) into Eq. (12), the following equation can be obtained:

$$C\frac{d\varphi}{dx} - C\frac{d^2 w}{dx^2} + k_e w - 2t_e\left(\frac{\partial^2 w}{\partial x^2}\right) = q \tag{13}$$

Eqs. (12) and (13) can be reduced to a single fourth-order ordinary differential equation of w:

$$\left(D + \frac{2Dt_e}{C}\right)\frac{d^4 w}{dx^4} - \left(\frac{k_e D}{C} + 2t_e\right)\frac{d^2 w}{dx^2} + k_e w = q - \frac{D}{C}\frac{d^2(q)}{dx^2} \tag{14}$$

The external pressure $q(x)$ can be expressed by a function of x ($0 < x < L$), using the Fourier cosine series as follows:

$$q(x) = A_0 + \sum_{n=1}^{n=\infty} A_n \cos\frac{n\pi}{L}x \tag{15}$$

where L = length of the calculation region, $A_0 = \frac{1}{L}\int_0^L q(x)dx$, $A_n = \frac{2}{L}\int_0^L f(x)\cos\left(\frac{n\pi x}{L}\right)dx$.

The general solution to the vertical displacement function, w, can be written as:

$$w = e^{\alpha x}(c_1\cos\beta x + c_2\sin\beta x) + e^{-\alpha x}(c_3\cos\beta x + c_4\sin\beta x) + \frac{A_0}{k_e} + \sum_{n=1}^{n=\infty} a_n\cos\frac{n\pi}{L}x \tag{16}$$

where c_1, c_2, c_3, and c_4 are constants which can be determined based on the boundary conditions; α, β, and a_n are as follows:

$$\alpha = \sqrt{\sqrt{\frac{k_e}{4(D + \frac{2Dt_e}{C})}} + \frac{\frac{k_e D}{C} + 2t_e}{4(D + \frac{2Dt_e}{C})}} \tag{17a}$$

$$\beta = \sqrt{\sqrt{\frac{k_e}{4(D + \frac{2Dt_e}{C})}} - \frac{\frac{k_e D}{C} + 2t_e}{4(D + \frac{2Dt_e}{C})}} \tag{17b}$$

$$a_n = \frac{A_n[1 + (\frac{n\pi}{L})^2\frac{D}{C}]}{(D + \frac{2Dt_e}{C})(\frac{n\pi}{L})^4 + (\frac{k_e D}{C} + 2t_e)(\frac{n\pi}{L})^2 + k_e} \tag{17c}$$

The above equation holds under the condition $\sqrt{\frac{k_e}{4(D + \frac{2Dt_e}{C})}} > \frac{k_e D + 2t_e C}{4(DC + 2Dt_e)}$; if $\sqrt{\frac{k_e}{4(D + \frac{2Dt_e}{C})}} \leqslant \frac{k_e D + 2t_e C}{4(DC + 2Dt_e)}$, then β in the equation should be substituted by $\beta = i\beta$.

The rotation angle function of the tunnel φ is expressed as

$$\varphi = e^{\alpha x}(c_5\cos\beta x + c_6\sin\beta x) + e^{-\alpha x}(c_7\cos\beta x + c_8\sin\beta x) + \sum_{n=1}^{n=\infty}\left\{\left[\frac{D}{C}\left(1 + \frac{2t_e}{C}\right)\left(\frac{n\pi}{L}\right)^3 - \left(1 - \frac{Dk_e}{C^2}\right)\left(\frac{n\pi}{L}\right)\right]a_n - \frac{n\pi D}{LC^2}A_n\right\}\sin\frac{n\pi}{L}x \tag{18}$$

where c_5, c_6, c_7, and c_8 are constants that can be calculated from c_1, c_2, c_3, and c_4.

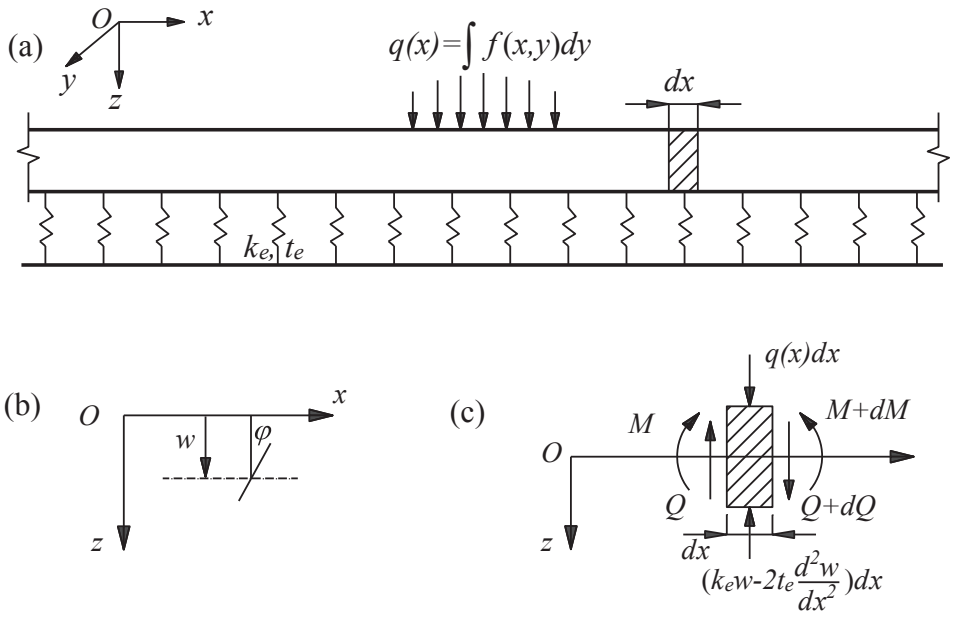

Fig. 5. Timoshenko beam model of tunnel on Winkler foundation: (a) schematic illustration of model; (b) displacement parameters and their positive directions; (c) beam element and forces.

$$c_5 = c_1\left[\alpha\left(1-\frac{Dk_e}{C^2}\right)+\frac{D}{C}\left(1+\frac{2t_e}{C}\right)(\alpha^3-3\alpha\beta^2)\right] + c_2\left[\beta\left(1-\frac{Dk_e}{C^2}\right)+\frac{D}{C}\left(1+\frac{2t_e}{C}\right)(3\alpha^2\beta-\beta^3)\right] \tag{19a}$$

$$c_6 = c_1\left[-\beta\left(1-\frac{Dk_e}{C^2}\right)+\frac{D}{C}\left(1+\frac{2t_e}{C}\right)(\beta^3-3\alpha^2\beta)\right] + c_2\left[\alpha\left(1-\frac{Dk_e}{C^2}\right)+\frac{D}{C}\left(1+\frac{2t_e}{C}\right)(\alpha^3-3\alpha\beta^2)\right] \tag{19b}$$

$$c_7 = c_3\left[-\alpha\left(1-\frac{Dk_e}{C^2}\right)+\frac{D}{C}\left(1+\frac{2t_e}{C}\right)(-\alpha^3+3\alpha\beta^2)\right] + c_4\left[\beta\left(1-\frac{Dk_e}{C^2}\right)+\frac{D}{C}\left(1+\frac{2t_e}{C}\right)(3\alpha^2\beta-\beta^3)\right] \tag{19c}$$

$$c_8 = c_3\left[-\beta\left(1-\frac{Dk_e}{C^2}\right)+\frac{D}{C}\left(1+\frac{2t_e}{C}\right)(\beta^3-3\alpha^2\beta)\right] + c_4\left[-\alpha\left(1-\frac{Dk_e}{C^2}\right)+\frac{D}{C}\left(1+\frac{2t_e}{C}\right)(-\alpha^3+3\alpha\beta^2)\right] \tag{19d}$$

The rate of the rotation angle, $\frac{d\varphi}{dx}$, is expressed as

$$\frac{d\varphi}{dx} = e^{\alpha x}(c_9\cos\beta x + c_{10}\sin\beta x) + e^{-\alpha x}(c_{11}\cos\beta x + c_{12}\sin\beta x) + \sum_{n=1}^{n=\infty}\left[-a_n\left(\frac{n\pi}{L}\right)^2\left(1+\frac{2t_e}{C}\right)-a_n\frac{k_e}{C}+\frac{1}{C}A_n\right]\cos\frac{n\pi}{L}x \tag{20}$$

Where

$$c_9 = c_1\left[(\alpha^2-\beta^2)\left(1+\frac{2t_e}{C}\right)-\frac{k_e}{C}\right]+2c_2\left(1+\frac{2t_e}{C}\right)\alpha\beta \tag{21a}$$

$$c_{10} = -2c_1\left(1+\frac{2t_e}{C}\right)\alpha\beta + c_2\left[(\alpha^2-\beta^2)\left(1+\frac{2t_e}{C}\right)-\frac{k_e}{C}\right] \tag{21b}$$

$$c_{11} = c_3\left[(\alpha^2-\beta^2)\left(1+\frac{2t_e}{C}\right)-\frac{k_e}{C}\right]-2c_4\left(1+\frac{2t_e}{C}\right)\alpha\beta \tag{21c}$$

$$c_{12} = 2c_3\left(1+\frac{2t_e}{C}\right)\alpha\beta + c_4\left[(\alpha^2-\beta^2)\left(1+\frac{2t_e}{C}\right)-\frac{k_e}{C}\right] \tag{21d}$$

If rate of the rotation angle is known, the bending moment, M, can be obtained using Eq. (2b) and Eq. (3a).

$$M = -D\frac{d\varphi}{dx} = -D\{e^{\alpha x}(c_9\cos\beta x + c_{10}\sin\beta x) + e^{-\alpha x}(c_{11}\cos\beta x + c_{12}\sin\beta x) + \sum_{n=1}^{n=\infty}\left[-a_n\left(\frac{n\pi}{L}\right)^2\left(1+\frac{2t_e}{C}\right)-a_n\frac{k_e}{C}+\frac{1}{C}A_n\right]\cos\frac{n\pi}{L}x\Big\} \tag{22}$$

The shear force, Q, is expressed as

$$Q = C\left(\frac{dw}{dx}-\varphi\right) = D\{e^{\alpha x}(c_{13}\cos\beta x + c_{14}\sin\beta x) + e^{-\alpha x}(c_{15}\cos\beta x + c_{16}\sin\beta x) + D\sum_{n=1}^{n=\infty}\left[-\left(1+\frac{2t_e}{C}\right)\left(\frac{n\pi}{L}\right)^3 a_n-\frac{k_e}{C}\left(\frac{n\pi}{L}\right)a_n+\frac{n\pi}{CL}A_n\right]\sin\frac{n\pi}{L}x\Big\} \tag{23}$$

where,

$$c_{13} = c_1\left[\alpha\frac{k_e}{C}-\left(1+\frac{2t_e}{C}\right)(\alpha^3-3\alpha\beta^2)\right]+c_2\left[\beta\frac{k_e}{C}-\left(1+\frac{2t_e}{C}\right)(3\alpha^2\beta-\beta^3)\right] \tag{24a}$$

$$c_{14} = c_1\left[-\beta\frac{k_e}{C}+\left(1+\frac{2t_e}{C}\right)(3\alpha^2\beta-\beta^3)\right]+c_2\left[\alpha\frac{k_e}{C}-\left(1+\frac{2t_e}{C}\right)(\alpha^3-3\alpha\beta^2)\right] \tag{24b}$$

$$c_{15} = c_3\left[-\alpha\frac{k_e}{C}+\left(1+\frac{2t_e}{C}\right)(\alpha^3-3\alpha\beta^2)\right]+c_4\left[\beta\frac{k_e}{C}-\left(1+\frac{2t_e}{C}\right)(3\alpha^2\beta-\beta^3)\right] \tag{24c}$$

$$c_{16} = c_3\left[-\beta\frac{k_e}{C}+\left(1+\frac{2t_e}{C}\right)(3\alpha^2\beta-\beta^3)\right] + c_4\left[-\alpha\frac{k_e}{C}+\left(1+\frac{2t_e}{C}\right)(\alpha^3-3\alpha\beta^2)\right] \tag{24d}$$

The constants c_1, c_2, c_3, and c_4 can be determined based on the boundary conditions. The boundary conditions can be different when location of the external force changes. Fig. 6 shows the boundary conditions for different location of the load application.

(a) Boundary condition I

As shown in Fig. 6(a), if the external force is added upon the middle part of the tunnel section, there will be no displacements and rotations in the two side of the model provided that the calculation length, L, is long enough to cover the influence range of the force. That is,

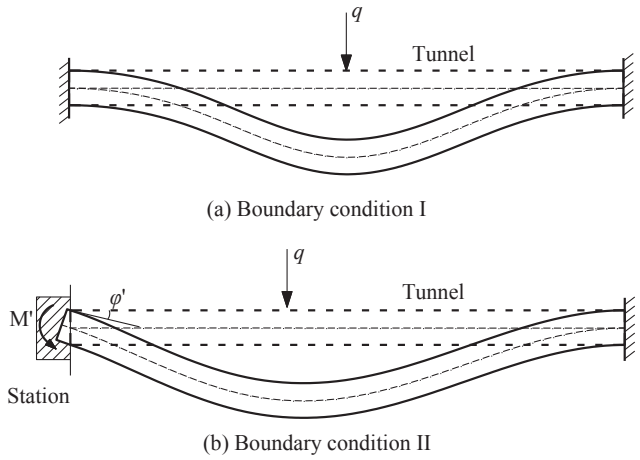

Fig. 6. Boundary conditions for different location of load application.

$$w|_{x=0}=0;\ \varphi|_{x=0}=0;\ w|_{x=L}=0;\ \varphi|_{x=L}=0 \tag{25a-b}$$

Using Eq. (16) for w and (18) for φ, we have

$$c_1+c_3=R_1 \tag{26a}$$

$$\begin{aligned}\text{where } R_1=&-\frac{A_0}{k_e}-\sum_{n=1}^{n=\infty}a_n\\ &c_1\left[\alpha\left(1-\frac{Dk_e}{c^2}\right)+\frac{D}{C}\left(1+\frac{2t_e}{C}\right)(\alpha^3-3\alpha\beta^2)\right]\\ &+c_2\left[\beta\left(1-\frac{Dk_e}{c^2}\right)+\frac{D}{C}\left(1+\frac{2t_e}{C}\right)(3\alpha^2\beta-\beta^3)\right]\\ &+c_3\left[-\alpha\left(1-\frac{Dk_e}{c^2}\right)+\frac{D}{C}\left(1+\frac{2t_e}{C}\right)(-\alpha^3+3\alpha\beta^2)\right]\\ &+c_4\left[\beta\left(1-\frac{Dk_e}{c^2}\right)+\frac{D}{C}\left(1+\frac{2t_e}{C}\right)(3\alpha^2\beta-\beta^3)\right]=0\end{aligned} \tag{26b}$$

$$c_1e^{\alpha L}\cos\beta L+c_2e^{\alpha L}\sin\beta L+c_3e^{-\alpha L}\cos\beta L+c_4e^{-\alpha L}\sin\beta L=R_3 \tag{26c}$$

$$\begin{aligned}\text{where } R_3=&-\frac{A_0}{k_sb}-\sum_{n=1}^{n=\infty}a_n\cos n\pi\\ &c_1\left\{\begin{array}{l}e^{\alpha L}\cos\beta L\left[\alpha\left(1-\frac{Dk_e}{c^2}\right)+\frac{D}{C}\left(1+\frac{2t_e}{C}\right)(\alpha^3-3\alpha\beta^2)\right]\\ +e^{\alpha L}\sin\beta L\left[-\beta\left(1-\frac{Dk_e}{c^2}\right)+\frac{D}{C}\left(1+\frac{2t_e}{C}\right)(-3\alpha^2\beta+\beta^3)\right]\end{array}\right\}\\ &+c_2\left\{\begin{array}{l}e^{\alpha L}\cos\beta L\left[\beta\left(1-\frac{Dk_e}{c^2}\right)+\frac{D}{C}\left(1+\frac{2t_e}{C}\right)(3\alpha^2\beta-\beta^3)\right]\\ +e^{\alpha L}\sin\beta L\left[\alpha\left(1-\frac{Dk_e}{c^2}\right)+\frac{D}{C}\left(1+\frac{2t_e}{C}\right)(\alpha^3-3\alpha\beta^2)\right]\end{array}\right\}\\ &+c_3\left\{\begin{array}{l}e^{-\alpha L}\cos\beta L\left[-\alpha\left(1-\frac{Dk_e}{c^2}\right)+\frac{D}{C}\left(1+\frac{2t_e}{C}\right)(-\alpha^3+3\alpha\beta^2)\right]\\ +e^{-\alpha L}\sin\beta L\left[-\beta\left(1-\frac{Dk_e}{c^2}\right)+\frac{D}{C}\left(1+\frac{2t_e}{C}\right)(-3\alpha^2\beta+\beta^3)\right]\end{array}\right\}\\ &+c_4\left\{\begin{array}{l}e^{-\alpha L}\cos\beta L\left[\beta\left(1-\frac{Dk_e}{c^2}\right)+\frac{D}{C}\left(1+\frac{2t_e}{C}\right)(3\alpha^2\beta-\beta^3)\right]\\ +e^{-\alpha L}\sin\beta L\left[-\alpha\left(1-\frac{Dk_e}{c^2}\right)+\frac{D}{C}\left(1+\frac{2t_e}{C}\right)(-\alpha^3+3\alpha\beta^2)\right]\end{array}\right\}\\ &=R_4\end{aligned} \tag{26d}$$

$$\text{Where } R_4=-\sum_{n=1}^{n=\infty}\left\{\left[\frac{D}{C}\left(1+\frac{2t_e}{C}\right)\left(\frac{n\pi}{L}\right)^3-\left(1-\frac{Dk_e}{c^2}\right)\left(\frac{n\pi}{L}\right)\right]a_n-\frac{n\pi D}{LC^2}A_n\right\}\sin n\pi$$

Eqs. (26) can be written in a matrix form

$$[M]\{c\}=\{R\} \tag{27}$$

where, $\{c\}=[c_1, c_2, c_3, c_4]^{-1}$, $\{R\}=[R_1, 0, R_3, R_4]^{-1}$. The coefficient M_{ij} $(i=1\cdots4, j=1\cdots4)$in $[M]$can be found from Eq. (24).

$$\{c\}=[M]^{-1}\{R\} \tag{28}$$

Once c_1, c_2, c_3, and c_4 are determined, w and φ can be calculated. Then, the internal forces of the tunnel can be obtained from Eqs. (22) and (23), and the opening of the joint and dislocation between rings can be calculated by Eqs. (9) and (10).

(b) Boundary condition II

If the external force is close to the station, a fixed boundary condition would be inapplicable at the joint between station and tunnel. Generally, the joint between station and tunnel in shield tunnels use a flexible connection which allows the tunnel to rotate to a certain degree (Wu et al., 2013). In this case, the boundary condition is shown in Fig. 6(b). Assume that the bending moment produced to resist rotation of the tunnel M', is linearly related to the rotation angle φ', that is, $M'=R_T\varphi'$, where R_T is rotational stiffness of the joint. Then the boundary condition in the two side of the model can be expressed as follows, provided that the calculation length, L, is long enough to cover the influence range of the force.

$$w|_{x=0}=0;\ M|_{x=0}=R_T\varphi;\ w|_{x=L}=0;\ \varphi|_{x=L}=0 \tag{29a-d}$$

Substituting Eqs. (18) and (22) into the boundary condition in Eq. (26b), yields

$$\begin{aligned}&c_1\left[\begin{array}{c}R_T\alpha\left(1-\frac{Dk_e}{c^2}\right)+\frac{DR_T}{C}\left(1+\frac{2t_e}{C}\right)(\alpha^3-3\alpha\beta^2)\\ +D\left((\alpha^2-\beta^2)\left(1+\frac{2t_e}{C}\right)-\frac{k_e}{C}\right)\end{array}\right]\\ &+c_2\left[R_T\beta\left(1-\frac{Dk_e}{c^2}\right)+\frac{DR_T}{C}\left(1+\frac{2t_e}{C}\right)(3\alpha^2\beta-\beta^3)+2D\alpha\beta\left(1+\frac{2t_e}{C}\right)\right]\\ &+c_3\left[\begin{array}{c}-R_T\alpha\left(1-\frac{Dk_e}{c^2}\right)+\frac{DR_T}{C}\left(1+\frac{2t_e}{C}\right)(-\alpha^3+3\alpha\beta^2)\\ +3D\left((\alpha^2-\beta^2)\left(1+\frac{2t_e}{C}\right)-\frac{k_e}{C}\right)\end{array}\right]\\ &+c_4\left[R_T\beta\left(1-\frac{Dk_e}{c^2}\right)+\frac{D}{C}\left(1+\frac{2t_e}{C}\right)(3\alpha^2\beta-\beta^3)-2D\alpha\beta\left(1+\frac{2t_e}{C}\right)\right]\\ &=R_2\end{aligned} \tag{30}$$

where, $R_2=D\sum_{n=1}^{n=\infty}\left[a_n\left(\frac{n\pi}{L}\right)^2+a_n\frac{k_e}{C}-\frac{A_n}{C}\right]$

Eqs. (26a), (30), (26c), (26d) can be written into the matrix form in Eq. (27), and the constants c_1, c_2, c_3, and c_4 for boundary condition II can be determined.

4. Case study and discussion

4.1. Formulation of the problem

To validate the effectiveness of the proposed model, a shield tunnel section in Shanghai Metro subjected to an external force transferred from surcharge load on the ground surface was analyzed. Fig. 7 shows an illustration of a shield tunnel subjected to surcharge load on the ground surface. The ground surface above the tunnel is subjected to a surcharge of 10 m × 10 m, and the load pressure, P, is 150 kPa. The length of the tunnel section between two stations is 1000 m. The buried depth of the tunnel is about 6 m. Table 1 shows the basic parameters of the segments and bolts of metro tunnels in Shanghai, which are obtained from Shen et al. (2014) and Liao et al. (2008). The shear

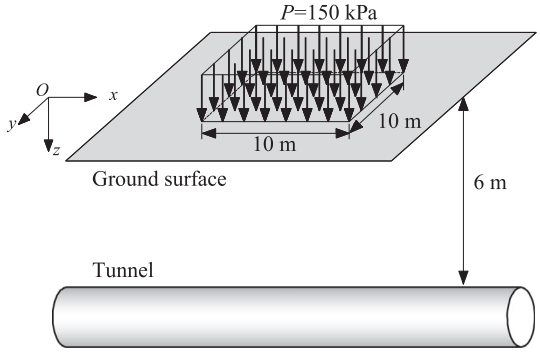

Fig. 7. Case study of a shield tunnel subjected to surcharge load on the ground surface.

Table 1
Parameters of segments and bolts used in metro tunnels in Shanghai.

Segmental rings		Bolts	
Outer diameter (mm)	6200	Number of circumferental bolts	12
Inner diameter (mm)	5500	Number of longitudinal bolts	17
Thickness (mm)	350	Diameter	30
Length (mm)	1000	Length (mm)	400
Young's modulus (kPa)	3.45×10^7	Young's modulus (kPa)	2.06×10^8
Shear modulus, G_s	1.4375×10^7	Shear modulus, G_s	7.923×10^7
Poisson's ratio, ν	0.2	Poisson's ratio, ν	0.3

modulus is calculated based on the following equation: $G_s = 0.5E/(1 + \nu)$. The metro tunnel has outer diameter of 6.2 m and inner diameter of 5.5 m. It consists of six precast reinforced concrete segments to form a ring. Each segmental ring is 1 m in length. The soil profile at the site is as follows. The upper deposit is a crust layer with a thickness of 3 m. Next is the typical first soft clay layer of Shanghai, which consists of a 3 m-thick, mucky, silty, clay layer and a 9.5 m-thick, mucky, clay layer. Under that is the second soft clay layer with a thickness of 20 m, and it is slightly stiffer than the first clay layer. The physical and mechanical properties of the soils can refer to the previous publications of authors (Shen and Xu, 2011; Shen et al., 2013, 2014; Ye et al., 2015). The Shanghai clay has the characteristics of high compressibility and high sensitivity with strong creep behavior (Yin et al., 2010, 2011; Yin and Chang, 2013). For the mucky clay layer, the elastic modulus E is 1.3 MPa and the Poisson's ratio ν is 0.35; for the underlying clay layer, the elastic modulus E is 2.3 MPa and the Poisson's ratio ν is 0.33 (SURCTC, 2012).

4.2. Analysis method

4.2.1. Foundation parameters

The compression modulus k and the shear modulus t of Vlasov foundation can be calculated based on the Elastic modulus and the Poisson's ratio of the soil (Vlasov and Leontev, 1966).

$$k = \frac{E_0}{1-\nu_0^2}\int_0^H [h'(z)]^2 dz \tag{31}$$

$$t = \frac{E_0}{4(1-\nu_0)}\int_0^H [h(z)]^2 dz \tag{32}$$

where, $E_0 = \frac{E_s}{1-\nu^2}$, $\nu_0 = \frac{\nu}{1-\nu}$, E_s = Elastic modulus of soil, ν = Poisson's ratio of soil. $h(z)$ = displacement variation function in vertical direction, which is expressed as:

$$h(z) = \frac{sh[\tau(H-z)/L_l]}{sh[\tau H/L_l]} \tag{33}$$

where, τ is constant, in general, $\tau = 1$; $L_l = \left[\frac{2(EI)_{eq}(1-\nu^2)}{E_s b}\right]^{\frac{1}{3}}$.

According to Eqs. (31)-(33), it is worked out that the compression modulus of Vlasov foundation $k = 5344.4\ \mathrm{kN/m^3}$, and the shear modulus of Vlasov foundation $t = 23485.6\ \mathrm{kN/m^3}$.

4.2.2. Load acting upon the tunnel

The pressure load acting upon the tunnel can be calculated using the method proposed by Boussinesq (1885). If the foundation is constructed in the location of 500 m from the studying point, the calculated pressure load is shown in Fig. 8(a). The pressure load is a function of two variables, $f(x, y)$. Integrating the function over y direction from −3.1 m to 3.1 m, the pressure load along the longitudinal direction, $q(x)$, can be obtained, as shown in Fig. 8(b). The $q(x)$ can be expressed by a Gaussian function:

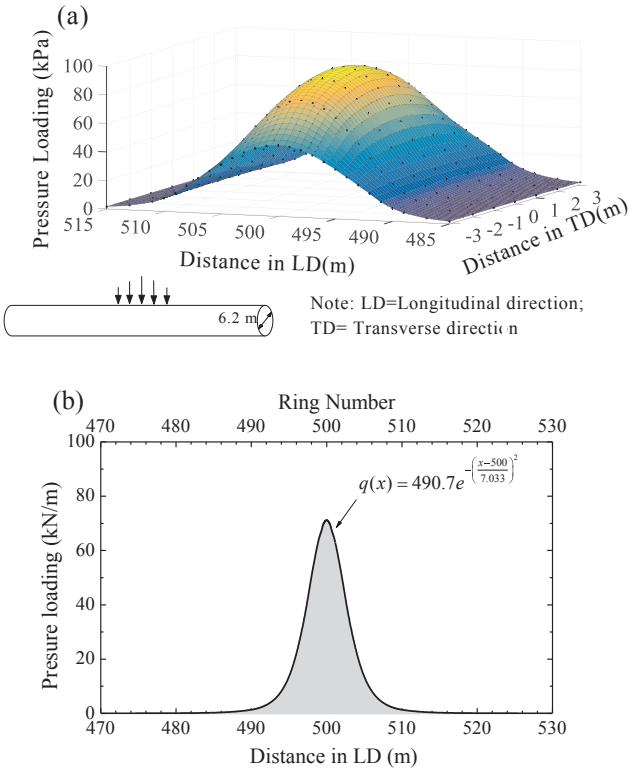

Fig. 8. Distribution of additional pressure loading on shield tunnel: (a) in both transverse and longitudinal direction; (b) in longitudinal direction.

$$q(x) = 490.7e^{-\left(\frac{x-500}{7.033}\right)^2} \tag{34}$$

It can be further expressed in a Fourier series as in Eq. (11).

4.2.3. Analysis cases

This study considers different locations of independent foundation above the tunnel: (*i*) on the middle part of the tunnel section (500 m from the starting point); (*ii*) near the station (10 m, 15 m, 20 m, 30 m, 40 m from the starting point). For the former case, the fixed boundary conditions shown in Eq. (25) can be adopted if the calculation length is 200 m. For the latter case, the boundary conditions shown in Eq. 26 can be adopted if the calculation range is set from the starting point to 200 m away.

According to Liao et al. (2008), the reduction factor for flexural stiffness of metro tunnels in Shanghai is $\eta = 1/7$. This equates to a flexural stiffness of the tunnel $(EI)_{eq}$ at $1.361 \times 10^8\ \mathrm{kN\,m^2}$. Research on the equivalent shear stiffness of shield tunnels of Shanghai is comparatively rare. According to Eq. (5), if the modified factor $\xi = 1$, the equivalent shear stiffness $(\kappa GA)_{eq}$ is $2.08 \times 10^6\ \mathrm{kN}$. In this study, a parameter study for the equivalent shear stiffness will be conducted, with different values for the modified factor $\xi = 2, 1, 0.5, 0.2, 0.1$. For comparison, both the proposed Timoshenko beam model and the traditional Euler-Bernoulli beam model on a Vlasov foundation was adopted.

The rotational stiffness of the joint between station and tunnel, R_T, depends on the construction technology. In engineering practices, different technologies have been applied, e.g. rigid connection by welding steel plate embedded in the segmental lining onto steel shaft ring; flexible connection by riveting the segmental lining on a steel plate, which allows the tunnel to rotate to a certain degree, and so on. Moreover, geohazards is easy to happen during shield tunneling in this ground (Lyu et al., 2018a,b) so that the soft soil outside station shaft is general need to be improved using jet grouting during underground construction (Shen et al., 2017). All of these factors affect the value of

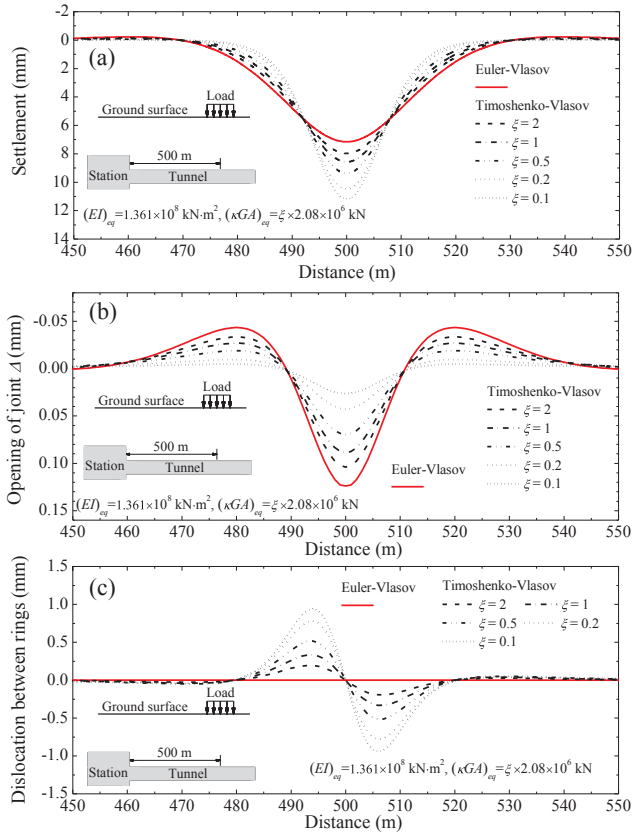

Fig. 9. Calculated deformation of the tunnel considering different equivalent shear stiffness: (a) settlement; (b) opening of joints; (c) dislocation between rings.

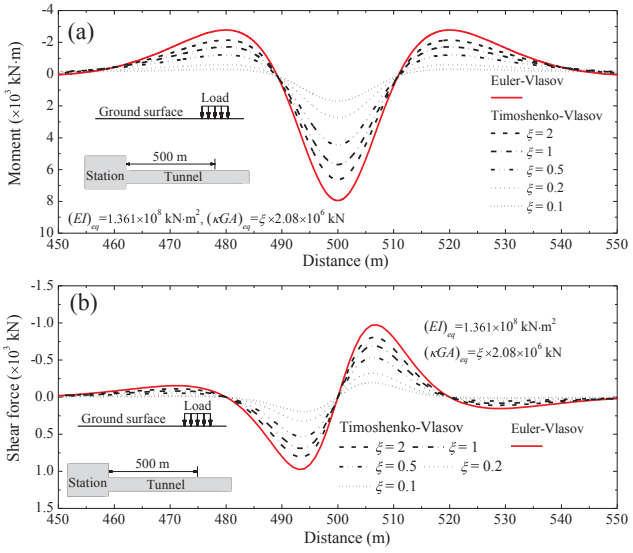

Fig. 10. Calculated internal forces of the tunnel considering different equivalent shear stiffness: (a) bending moment; (b) shear force.

rotational stiffness. However, there is no research on the calculation of rotational stiffness found. In this study, a parameter study on the rotational stiffness was conducted, by assuming $R_T = 1.0 \times 10^6$ kN m/rad, 1.0×10^5 kN m/rad, 1.0×10^4 kN m/rad, and the effect of R_T on the tunnel behavior was investigated. In the following discussion, the rotation obtained from the assumption of R_T is within the allowance of the current technology. However, further investigation on the rotation stiffness is necessary in the future.

4.3. Results and discussion

4.3.1. Effect of equivalent shear stiffness

When the independent foundation is constructed in the middle of the tunnel section (500 m from the starting point), the calculated tunnel deformation considering different modified factor of equivalent shear stiffness is shown in Fig. 9. Typical aspects of tunnel deformation, such as settlement, maximum opening of joints, and dislocation between rings are investigated. As shown in Fig. 9(a), the tunnel settlement trough obtained from the Timoshenko beam model was greater and narrower than that calculated by the Euler-Bernoulli model. This is because the Timoshenko model allows shear deformation of the tunnel, which makes the load-bearing ability of the tunnel smaller than that of the Euler-Bernoulli model. With a smaller load-bearing ability, the effect of an acting load tends to limit in the loaded region. When the modified factor $\xi = 1$, the maximum settlement of the tunnel is 8 mm, and the influencing diameter, within which the displacement of tunnel is less than 0.1 mm, is about 45 m.

Despite a smaller settlement occurring, the Euler-Bernoulli model predicts a greater opening of joints than the Timoshenko model, as shown in Fig. 9(b); and there is no dislocation between rings for Euler-Bernoulli beam model, as depicted in Fig. 9(c). For Timoshenko model, with the decrease of the equivalent shear stiffness, the depth of the settlement trough increases, the opening of the joint decreases, and the dislocation between rings increases. If the shear stiffness is great enough, the Timoshenko model will degenerate into an Euler-Bernoulli model. When the modified factor $\xi = 1$, the maximum opening of the joint is 0.1 and the dislocation is 0.2 mm. If great settlement occurred, failure of the bolts in circumferential joints can be caused, which will greatly reduce the shear stiffness of the joint. The shearing dislocation will become the main deformation mode of the tunnel.

Fig. 10(a) and (b) compares the moment and the shear force of a tunnel calculated using the proposed model with those calculated using the traditional Euler model. It can be found that Timoshenko model predicts a smaller moment and force than the Euler model although the magnitude of tunnel settlement is greater than that of Euler model. The results indicate that the Euler-Bernoulli beam model underestimates the tunnel deformation and overestimates the internal forces. With the decrease in the shear stiffness, the internal force decreases gradually, despite of a greater deformation is caused.

4.3.2. Effect of location of load application

Assume the surcharge load is acted close to the station, with a distance L_f equating to 10 m, 15 m, 20 m, 30 m, 40 m, respectively. The rotational stiffness of the joint between station and tunnel, R_T, is assumed as 1.0×10^6 kN m/rad, and the equivalent shear stiffness, $(\kappa GA)_{eq}$, is assumed as 2.08×10^6 kN. Since the distance between the foundation and the station is less than the influencing diameter of 45 m, the settlement behavior of the tunnel should be calculated using boundary condition II. Fig. 11 shows the calculated deformation of the tunnel for different cases. It can be seen that, with the decrease of the distance between the load and the station, there is a slightly decrease of the maximum settlement of the tunnel. However, the maximum dislocation between segmental rings increases, which leads to a higher possibility of water leakage. Fig. 12 shows the calculated internal forces of the tunnel for different cases. It can be seen that there is no obvious change on the maximum bending moment, however, the shear force increases significantly with the decrease of distance between the load and the station.

4.3.3. Effect of the rotational stiffness of the joint between tunnel and station

Assume the independent foundation is located at 20 m from the station, and the equivalent shear stiffness, $(\kappa GA)_{eq}$, of the tunnel is

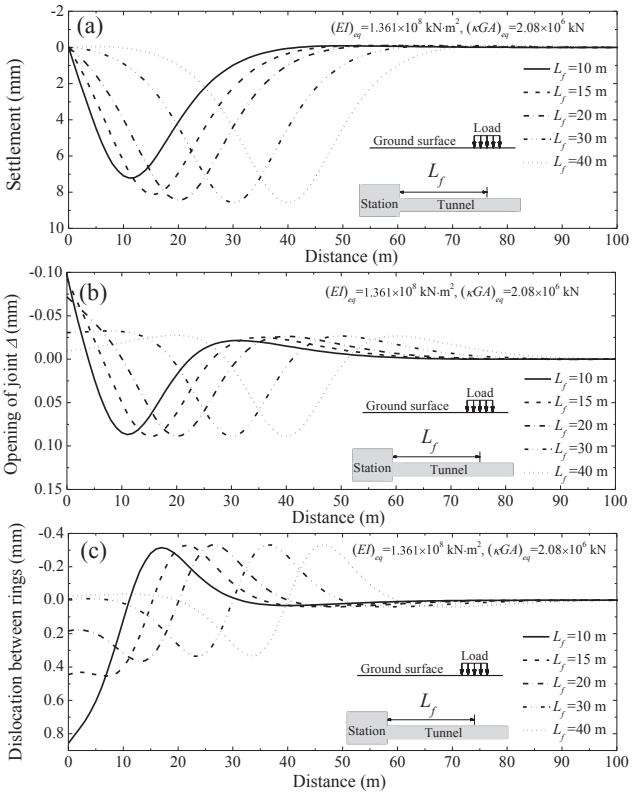

Fig. 11. Calculated deformation of the tunnel considering different location of load: (a) settlement; (b) opening of joints; (c) dislocation between rings.

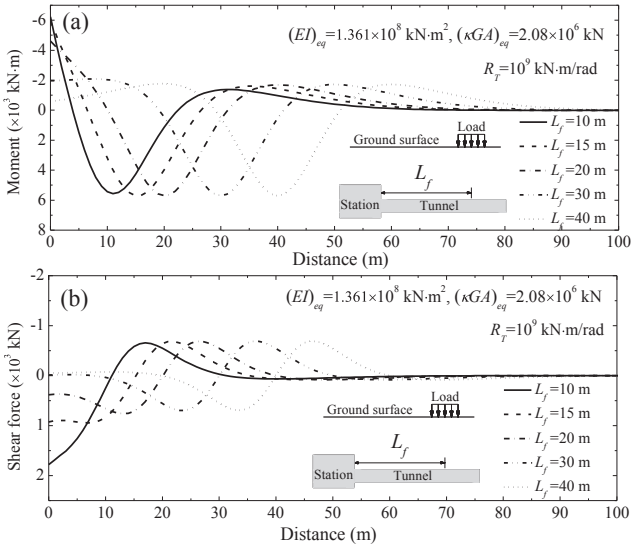

Fig. 12. Calculated internal forces of the tunnel considering different location of load: (a) bending moment; (b) shear force.

2.08 × 10^6 kN. Considering different rotational stiffness of the joint between tunnel and station (R_T = 1.0 × 10^6, 1.0 × 10^5, 1.0 × 10^4 kN·m/rad), the calculated deformation and internal forces of the tunnel is shown in Figs. 13 and 14. It can be seen that, with the decrease of R_T, the rotation angle of joint between tunnel and station increases gradually, and the maximum settlement of the tunnel increases slightly. A stiffer joint between tunnel and station will lead to a greater internal forces locally .

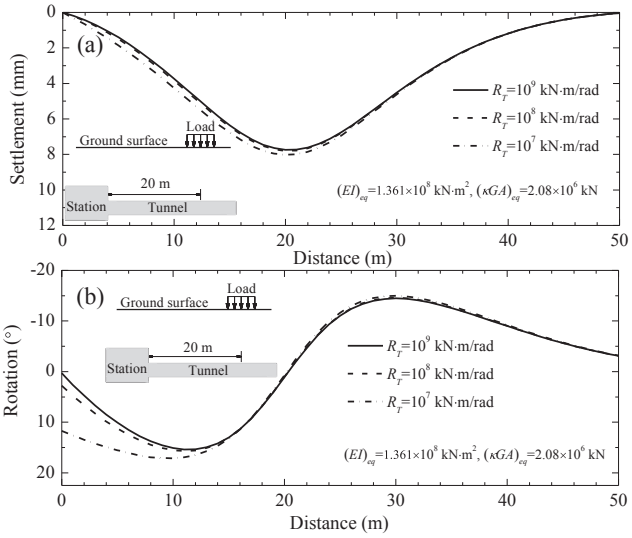

Fig. 13. Calculated deformation of the tunnel with different rotation stiffness at the joint between station and tunnel: (a) settlement; (b) rotation angle.

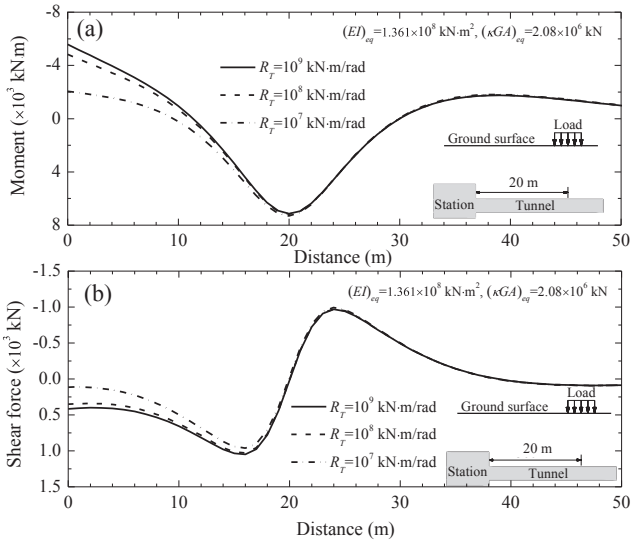

Fig. 14. Calculated internal forces of the tunnel with different rotation stiffness at the joint between station and tunnel: (a) bending moment; (b) shear force.

5. Conclusions

This paper presents the analytical model of soil-tunnel interaction for shield tunnels with consideration of shearing dislocation between segmental rings. The following conclusions can be drawn.

(a) The interaction between shield tunnel and soil can be simplified as a Timoshenko beam simplified model (TBSM) on Vlasov foundation with equivalent flexure stiffness $(EI)_{eq}$ and shear stiffness $(\kappa GA)_{eq}$. The model considers two boundary conditions: (i) fix boundary condition; (ii) allowing rotation in the boundary, therefore, can analyze the behavior of tunnel subjected to a load either in the middle of the tunnel section or close to the station in an appropriate way.

(b) Compared with TBSM on Vlasov foundation, the traditional model of Euler-Bernoulli beam predicts a smaller and wider settlement trough of the tunnel with significantly higher internal forces. That is, the Euler-Bernoulli beam model underestimates the tunnel deformation and overestimates the internal forces. With the decrease of shear stiffness, smaller rotation angles of the segmental rings

with smaller opening of joints and greater dislocation between rings are predicted.

(c) If the applied load is close to the station, with the decrease of the distance between the load and the station, there is a slightly decrease of the maximum settlement of the tunnel, but the maximum internal forces and the maximum joint deformation increases, which leads to a higher possibility of water leakage. A stiffer joint between tunnel and station will lead to a smaller maximum settlement of the tunnel, but cause a greater internal forces locally.

Acknowledgement

The research work described herein was funded by the National Nature Science Foundation of China (NSFC) (Grant No. 51508323) and the National Basic Research Program of China (973 Program: 2015CB057806). These financial supports are gratefully acknowledged.

References

Bogaards, P.J., Bakker, K.J., 1999. Longitudinal bending moments in the tube of a bored tunnel. In: Numerical Models in Geomechanics. Numog VII, Graz, Austria, pp. 317–321.

Boussinesq, M.J., 1885. Application des potentiels a l'etude de l'equilibre et du mouvement des solides elastiques, principalement au calcul des deformations et des pressions que produisent, dans ces solides, des efforts quelconques exerces sur une petite partie de leur surface ou de leur interieur: Memoire suivi de notes etendues sur divers points de physique mathematique et d'analyse. GauthierVillars, Paris, pp. 722.

Chai, J.C., Shen, J.S., Liu, M.D., Yuan, D.J., 2018. Predicting performance of embankments on PVD improved subsoils. Comput. Geotech. 93, 222–231. http://dx.doi.org/10.1016/j.compgeo.2017.05.018.

Cheng, W.C., Ni, J.C., Shen, S.L., 2017a. Experimental and analytical modeling of shield segment under cyclic loading. International Journal of Geomechnics, ASCE 17 (6). http://dx.doi.org/10.1061/(ASCE)GM.1943-5622.0000810.

Cheng, W.C., Ni, J.C., Shen, J.S., Huang, H.W., 2017b. Investigation into factors affecting jacking force: a case study. Geotech. Eng., ICE Proc. 170 (4), 322–334. http://dx.doi.org/10.1680/jgeen.16.00117.

Han, J., Frost, J.D., 2000. Load-deflection response of transversely isotropic piles under lateral loads. Int. J. Numer. Anal. Meth. Geomech. 24, 509–529.

Hetenyi, M., 1946. Beams on Elastic Foundations. University of Michigan Press, Ann Arbor, Michigan.

Huang, X., Huang, H.W., Zhang, J., 2012. Flattening of jointed shield-driven tunnel induced by longitudinal differential settlements. Tunn. Undergr. Sp. Technol. 31, 20–32.

Huang, H.W., Gong, W.P., Khoshnevisan, S., Juang, C.H., Zhang, D.M., Wang, L., 2015. Simplified procedure for finite element analysis of the longitudinal performance of shield tunnels considering spatial soil variability in longitudinal direction. Comput. Geotech. 64, 132–145.

ITA (Working Group No 2), 2000. Guidelines for the design of shield tunnel lining. Tunn. Undergr. Sp. Technol. 15 (3), 303–331.

Jin, Y.F., Yin, Z.Y., Shen, S.L., Hicher, P.Y., 2016. Selection of sand models and identification of parameters using an enhanced genetic algorithm. Int. J. Numer. Anal. Meth. Geomech. 40 (8), 1219–1240.

Jin, Y.F., Wu, Z.X., Yin, Z.Y., Shen, J.S., 2017. Estimation of critical state-related formula in advanced constitutive modeling of granular material. Acta Geotech. 12 (6), 1329–1351.

Koizumi, J., Murakami, H., Saino, K., 1988. Modelling of longitudinal structure of shield tunnel. J. Jpn. Soc. Civil Eng. 79–88 (in Japanese).

Li, P., Du, S.J., Shen, S.L., Wang, Y.H., Zhao, H.H., 2016. Timoshenko beam solution for the response of existing tunnels because of tunneling underneath. Int. J. Numer. Anal. Meth. Geomech. 40 (5), 766–784.

Liao, S.M., Peng, F.L., Shen, S.L., 2008. Analysis of shearing effect on tunnel induced by load transfer along longitudinal direction. Tunn. Undergr. Space. Technol. 23 (4), 421–430.

Liu, X.X., Shen, S.L., Xu, Y.S., Yin, Z.Y., 2018. Analytical approach for time-dependent groundwater inflow into shield tunnel face in confined aquifer. Int. J. Numer. Anal. Meth. Geomech. 42 (4), 655–673. http://dx.doi.org/10.1002/nag.2760.

Lyu, H.M., Sun, W.J., Shen, S.L., Arulrajah, A., 2018a. Flood risk assessment in metro systems of mega-cities using a GIS-based modeling approach. Sci. Total Environ. 626, 1012–1025. http://dx.doi.org/10.1016/j.scitotenv.2018.01.138.

Lyu, H.M., Shen, J.S., Arulrajah, A., 2018b. Assessment of Geohazards and preventive countermeasures using AHP incorporated with GIS in Lanzhou, China. Sustainability 10 (2), 304. http://dx.doi.org/10.3390/su10020304.

Mair, R.J., Taylor, R.N., 1997. Bored tunneling in the urban environment. State-of-the-art report and theme lecture. In: Proc. 14th Int. Conf. Soil Mech. Found. Engng, Hamburg, vol. 4, pp. 2353–2380.

Mair, R.J., 2008. Tunnelling and geotechnics: New horizons. Géotechnique 58 (9), 695–736.

Pasternak, P.L., 1954. On a new method of analysis of an elastic foundation by means of two foundation constants. Gosudatstvennoe Lzdatelgtro Liberaturi po Stroiterlstvui Arkhitekture, Moscow (in Russian).

SURCTC (Shanghai Urban and Rural Construction and Transportation Commission), 2012. DGJ08-37-2012: Code for investigation of geotechnical engineering. SURCTC, Shanghai, People's Republic of China.

Ren, D.J., Shen, S.L., Arulrajah, A., Wu, H.N., 2018. Evaluation of ground loss ratio induced in DOT tunnelling induced by moving trajectories. Can. Geotech. J., published online. http://dx.doi.org/10.1139/cgj-2017-0355.

Shen, S.L., Cui, Q.L., Ho, E.C., Xu, Y.S., 2016. Ground response to multiple parallel Micro tunneling operations in cemented silty clay and sand. J. Geotech. Geoenviron. Eng. 142, 04016001.

Shen, S.L., Xu, Y.S., 2011. Numerical evaluation of land subsidence induced by groundwater pumping in Shanghai. Can. Geotech. J. 48 (9), 1378–1392.

Shen, S.L., Ma, L., Xu, Y.S., Yin, Z.Y., 2013. Interpretation of increased deformation rate in aquifer IV due to groundwater pumping in Shanghai. Can. Geotech. J. 50 (11), 1129–1142.

Shen, S.L., Wu, H.N., Cui, Y.J., Yin, Z.Y., 2014. Long-term settlement behaviour of metro tunnels in the soft deposits of Shanghai. Tunneling Underground Space Technol. 40 (1), 309–323.

Shen, S.L., Wang, J.P., Wu, H.N., Xu, Y.S., 2015. Evaluation of hydraulic conductivity for both marine and deltaic deposits based on piezocone testing. Ocean Eng. 110, 174–182. http://dx.doi.org/10.1016/j.oceaneng.2015.10.011.

Shen, S.L., Wang, Z.F., Cheng, W.C., 2017. Estimation of lateral displacement induced by jet grouting in clayey soils. Geotechnique, ICE 167 (7), 621–630.

Shiba, Y., Kawashima, K., Ohikata, M., Kana, M., 1988. Evaluation of longitudinal structural stiffness of shield tunnel under earthquake loading. J. Jpn. Soc. Civil Eng. 385–394 (in Japanese).

Talmon, A.M., Bezuijen, A., 2013. Calculation of longitudinal bending moment and shear force for Shanghai Yangtze river tunnel: application of lessons from Dutch research. Tunn. Undergr. Sp. Technol. 35, 161–171.

Timoshenko, S.P., 1921. On the correction for shear of the differential equation for transverse vibration of prismatic bars. Philo. Mag 41, 744.

Vlasov, V.Z., Leontev, U.N., 1966. Beams, plates and phells on elastic foundations. Israel Program for Scientific Translations, Jerusalem (in Russian).

Wang, R.L., 2009. Analysis on the longitudinal deformation of shield tunnel of Shanghai metro. Underground Eng. Tunnels 4, 1–6 (in Chinese).

Winkler, E., 1867. Die Lehre von der Elastizitat and Feistigkeit. H. Dominicus, Prague, Czechoslovakia.

Wu, H.N., Huang, R.Q., Sun, W.J., Shen, S.L., Xu, Y.S., Liu, Y.B., Du, S.J., 2013. Leaking behaviour of shield tunnels under the Huangpu River of Shanghai with induced hazards. Nat. Hazards 70 (2), 1115–1132.

Wu, H.N., Shen, S.L., Liao, S.M., Yin, Z.Y., 2015. Longitudinal structural modelling of shield tunnels considering shearing dislocation between segmental rings. Tunneling Underground Space Technol. 50, 317–323.

Wu, H.N., Shen, S.L., Yang, J., 2017. Identification of tunnel settlement caused by land subsidence in soft deposit of Shanghai. J. Perform. Constructed Facilities, ASCE 31 (6), 04017092.

Ye, G.L., Hashimoto, T., Shen, S.L., Zhu, H.H., Bai, T.H., 2015. Lessons learnt from unusual ground settlement during Double-O-Tube tunnelling in soft ground. Tunn. Undergr. Sp. Technol. 49, 79–91.

Yin, J.H., 2000a. Comparative modeling study of reinforced beam on elastic foundation. J. Geotech. Geoenviron., ASCE 126 (3), 265–271.

Yin, J.H., 2000b. Close-form solution for reinforced Timoshenko beam on elastic foundation. J. Eng. Mech. 126 (8), 868–874.

Yin, Z.Y., Karstunen, M., Chang, C.S., Koskinen, M., Lojander, M., 2011. Modeling time-dependent behavior of soft sensitive clay. J. Geotech. Geoenviron. Eng. 137 (11), 1103–1113.

Yin, Z.Y., Chang, C.S., 2013. Stress-dilatancy behavior for sand under loading and unloading conditions. Int. J. Numer. Anal. Meth. Geomech. 37 (8), 855–870.

Yin, Z.Y., Chang, C.S., Karstunen, M., Hicher, P.Y., 2010. An anisotropic elastic viscoplastic model for soft clays. Int. J. Solids Struct. 47 (5), 665–677.

Yin, Z.Y., Jin, Y.F., Shen, J.S., Hicher, P.Y., 2018. Optimization techniques for identifying soil parameters in geotechnical engineering: Comparative study and enhancement. Int. J. Numer. Anal. Meth. Geomech. 42 (2), 70–94. http://dx.doi.org/10.1002/nag.2714.

Zhang, N., Shen, J.S., Zhou, A.N., Arulrajah, A., 2018. Tunneling induced geohazards in mylonite rock fault with rich groundwater: A case study in Guangzhou. Tunneling Underground Space Technol. 74, 262–272. http://dx.doi.org/10.1016/j.tust.2017.12.021.